Nondegenerate Two- and Three-Photon Nonlinearities in Semiconductors

Matthew Reichert[a,b], Peng Zhao[a], Himansu S. Pattanaik[a],
David J. Hagan[a,c], and Eric. W. Van Stryland[a,c]*
[a]CREOL, College of Optics and Photonics, University of Central Florida, Orlando, Florida 32816, USA; [b]Current address: Department of Electrical Engineering, Princeton University, Princeton, New Jersey 08455, USA; [c]Department of Physics, University of Central Florida, Orlando, Florida 32816, USA; *ewvs@creol.ucf.edu

ABSTRACT

Two-photon absorption, 2PA, in semiconductors is enhanced by two orders of magnitude due to intermediate-state resonance enhancement, ISRE, for very nondegenerate (ND) photon energies. Associated with this enhancement in loss is enhancement of the nonlinear refractive index, n_2. Even larger enhancement of three-photon absorption is calculated and observed. These large nonlinearities have implications for applications including ND two-photon gain and two-photon semiconductor lasers. Calculations for enhancement of ND-2PA in quantum wells is also presented showing another order of magnitude increase in 2PA. Potential devices include room temperature gated infrared detectors for LIDAR and all-optical switches.

Keywords: Nonlinear Optics, Semiconductors, Multiphoton Absorption, Quantum Wells

1. INTRODUCTION

There are many potential practical applications of optical nonlinearities in condensed matter, including all-optical switching [1-4], optical limiting [5, 6], sensing [7, 8], and imaging [9, 10]. Additionally, these same nonlinearities limit the performance, particularly in optical telecommunication, and can lead to unwanted absorption or even damage of solid-state devices [11]. The study of two-photon absorption (2PA) is instrumental in investigating material properties, since two-photon transitions are subject to a set of selection rules that are distinct from those governing one-photon transitions [12]. Furthermore, nonlinear refraction (NLR) is related to nondegenerate 2PA though Kramers-Kronig relations [13], and NLR causes effects such as self-focusing, self- and cross-phase modulation and four-wave mixing [14, 15], each of them having a number of practical applications. Therefore, precise knowledge of the nonlinear optical properties of semiconductor materials is of great practical importance. While there has been much theoretical and experimental work done on degenerate, or self-, nonlinearities, where only a single beam of a particular wavelength interacts with a material, nondegenerate nonlinear interactions are much less explored. In this work, we discuss recent theoretical and experimental progress on the understanding of nondegenerate nonlinearities in both bulk semiconductor and semiconductor quantum wells.

The principle nonlinear interactions of interest are nonlinear refraction and nonlinear absorption (namely two- and three-photon absorption), which result in changes in refractive index and absorption coefficient due the presence of a strong optical field. The material's response depends on its electronic energy levels, as well as the transition dipole moments between them. Knowledge of the wave functions and their energy levels thus allows prediction of the two-photon absorption coefficient α_2 and the nonlinear refractive index n_2. Alternatively, measurement of n_2 and α_2 provide information about the electronic energy levels and wave functions of a material.

Two-photon absorption, for example, depends on the initial, final, and intermediate states involved in the interactions. Figure 1(a) shows a simple three level model of the electronic states of a material, including an initial state i, final state f, and intermediate state j. The 2PA coefficient may occur for two photons when $\hbar\omega_a + \hbar\omega_b = E_{fi}$, and depends on the detuning with respect to the intermediate state $\Delta E_a = E_{ji} - \hbar\omega_a$ [16]

Ultrafast Bandgap Photonics, edited by Michael K. Rafailov, Eric Mazur, Proc. of SPIE Vol. 9835, 98350A · © 2016 SPIE
CCC code: 0277-786X/16/$18 · doi: 10.1117/12.2223286

$$\alpha_2(\omega_a;\omega_b) \propto \left| \frac{M_{fj}^{(b)} M_{ji}^{(a)}}{\Delta E_a} + \frac{M_{fj}^{(a)} M_{ji}^{(b)}}{\Delta E_b} \right|^2, \tag{1}$$

where the frequency arguments indicate irradiance loss of field *a* due to the presence of field *b*, and $M_{nm}^{(c)}$ is the matrix element coupling states *n* and *m* by the field *c* = *a*, *b*. As either photon energy becomes close to the energy difference between initial and intermediate states E_{ji}, $\alpha_2(\omega_a; \omega_b)$ is greatly enhanced, an effect known as intermediate state resonance enhancement (ISRE). In semiconductors, the intermediate states involved in the transition are within the conduction and valence bands themselves, meaning E_{ji} is either near the band-gap energy or near zero, respectively (see Figure 1(b)). In this case, ISRE occurs when one photon energy becomes close to the band-gap energy, $\hbar\omega_a \rightarrow E_g$, and the other goes towards zero, $\hbar\omega_b \rightarrow 0$. Thus, the largest enhancement occurs when the photon energies are very different from one another, so called extremely nondegenerate (END) enhancement. Similar enhancement is investigated here theoretically for semiconductor quantum wells [17], as well as for three-photon absorption in bulk semiconductors.

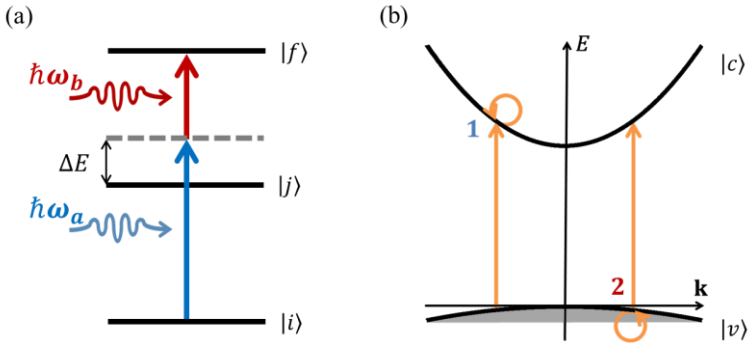

Figure 1. 2PA process in perturbation theory. (a) Three-level model showing one pathway of 2PA using the intermediate state *j*, where the absorption probability depends on the detuning Δ*E*. (b) In semiconductors the dominant pathways involve intermediate states within (1) conduction and (2) valence bands themselves, giving intermediate state resonance enhancement for extremely nondegenerate photon pairs.

This nondegenerate enhancement also applies to nonlinear refraction (NLR). ND-NLR is the refractive index change at frequency ω_a caused by the presence of a beam at frequency ω_b. The knowledge of the magnitude, sign and dispersion of the Kerr index $n_2(\omega_a; \omega_b)$ is critical for applications utilizing cross-phase modulation, such as optical switching [4]. Compared to degenerate NLR, ND-NLR is less often investigated experimentally, particularly for the END case and the spectral region where 2PA is present [18]. The theory is based on Kramers-Kronig transformation of the nondegenerate nonlinear absorption spectrum, where two-photon absorption (2PA), electronic Raman and optical Stark effect are taken into account [16, 18]. In this work, we have studied several direct-gap semiconductors using our nonlinear beam deflection technique [19]. The magnitudes and nonlinear dispersion of $n_2(\omega_a; \omega_b)$ are resolved over a broad spectral range with high nondegeneracy. We found agreement between our experimental results and theoretical predictions.

2. NONDEGENERATE TWO- AND THREE-PHOTON ABSORPTION

2.1 Nondegenerate Enhancement of 2PA

Two-photon absorption in bulk semiconductors can be greatly enhanced by ISRE using END photon pairs, which has been shown both theoretically [16] and experimentally [20]. For a two parabolic band model, the 2PA coefficient has been shown to follow

$$\alpha_2(\omega_a;\omega_b) = K \frac{\sqrt{E_p}}{n_a n_b E_g^3} F_2\left(\frac{\omega_a}{E_g}; \frac{\omega_b}{E_g}\right), \tag{2}$$

where

$$F_2\left(\frac{\omega_a}{E_g};\frac{\omega_b}{E_g}\right)=\frac{(x_a+x_b-1)^{3/2}}{2^7 x_a x_b^2}\left(\frac{1}{x_a}+\frac{1}{x_b}\right)^2, \tag{3}$$

and K = 3100 cm GW^{-1} eV$^{5/2}$, E_p is the Kane energy parameter, n_a and n_b are the linear refractive indices, and E_g is the bandgap energy. This enhancement has been measured for nondegeneracies as large as $\hbar\omega_a/\hbar\omega_b$ ~ 10 showing enhancement factors of up to 270 in ZnO over the degenerate case [20]. Such large enhancement factors suggests the use of END 2PA may be of practical use in applications. Gated detection of mid-IR pulses using END-2PA in p-i-n photodiodes have demonstrated greater sensitivity than liquid nitrogen cooled HgCdTe detectors [7]. This detection scheme has recently been used for 3D IR imaging [9], where the (nearly) instantaneous nature of the process ensures detection only when the two pulses are incident on the diode simultaneously. Depth information from reflective objects is encoded in the arrival time of the pulse to the detector, which only provides a signal when the gate pulse is synchronized, allowing for precise surface profile measurements.

Additionally, two-photon gain (2PG), which is the inverse process of 2PA, is likewise enhanced when using nondegenerate photons. 2PG is the stimulated emission of two photons, which is the two-photon analog to traditional stimulated emission. The 2PG coefficient is related to the 2PA coefficient by the inversion factor

$$\gamma_2(\omega_a;\omega_b)=\alpha_{2,0}(\omega_a;\omega_b)\left(f_c-f_v\right), \tag{4}$$

where $\alpha_{2,0}$ is the 2PA coefficient at equilibrium, and f_c and f_v are the Fermi-Dirac distributions of conduction and valence bands, respectively. Thus two-photon gain is enhanced whenever 2PA is enhanced, as shown in Figure 2. ND-2PG has recently been experimentally demonstrated in optically excited GaAs, using pump-probe techniques, demonstrating such enhancement [21]. END-2PG holds potential for the creation of a two-photon semiconductor laser.

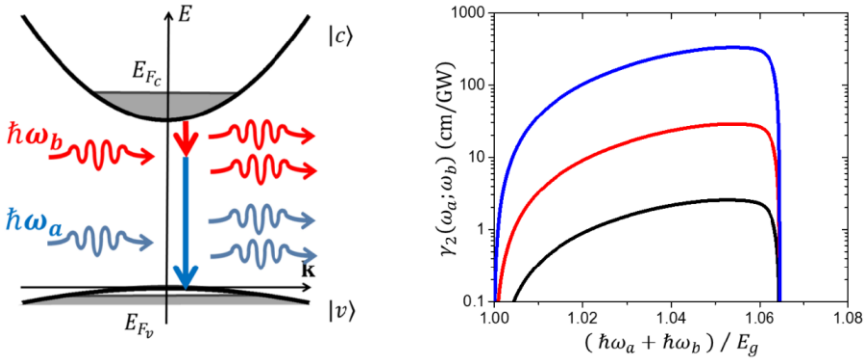

Figure 2. (left) E-k diagram showing 2PG. (right) 2PG spectra in GaAs for various nondegeneracy factors for GaAs at T = 20 K, N = 2×10^{18} cm^{-3} for (black) degenerate, (red) $\hbar\omega_b = 0.2E_g$, and (blue) $\hbar\omega_b = 0.1E_g$.

2.2 Nondegenerate 2PA in Quantum Wells

While degenerate (D) 2PA of quantum wells (QW's) has been studied by many groups [22-24], the nondegenerate regime has not been explored. The ND-2PA in QW's is expected to be enhanced more near the band edge as the density of states and the transition matrix elements exceed those of bulk semiconductors [17]. Since QW's are anisotropic, the 2PA selection rules differ for the electric field polarized in the plane of the QW's (TE) and light polarized perpendicular to the plane of the QW's (TM). Figure 3(a) shows a finite QW structure with the electric vector polarization for TE and TM cases. The transition paths for the 2PA in the TE-TE case is shown in Figure 3(b). The selection rules in the TE-TE case transitions are necessarily interband-intraband where the initial and final states are within valence and conductions bands of the same subband index n, respectively, i.e., $\Delta n = 0$. For the TM-TM case (i.e., both photons TM polarized) the selection rules are different and Δn must be odd. Thus the "interband" transition goes from a valence subband to a conduction subband, and the "intraband" transition occurs between two subbands within either the conduction or valence bands themselves. Thus, TM-TM 2PA transitions are interband-intersubband, as shown in Figure 3(c).

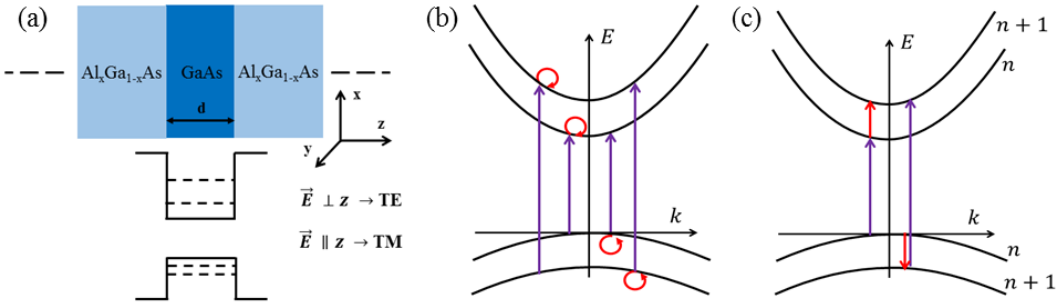

Figure 3. (a) Sketch of a QW structure with polarization for TE and TM cases. (b) Interband-intraband transitions for two TE polarized photons, and (c) interband-intersubband transitions for two TM polarized photons.

For the ND-2PA, an analytic expression is derived using second order perturbation theory both for TE-TE and TM-TM polarizations [17], which assumes an infinite QW. The ND-2PA coefficient for the TE-TE polarized case is

$$\alpha_{2,||}(\omega_a;\omega_b)=\frac{8\alpha^2 E_p\left(E_{lh,11}\right)^2\mu_{lh,\perp}\,d}{n_a n_b m_0 E_g^5}\left[\frac{1}{4}\frac{\mu_{lh,\perp}}{\mu_{hh,\perp}}F(\zeta_{hh})+\frac{1}{12}F(\zeta_{lh})\right]\frac{1}{(\omega_a/E_g)(\omega_b/E_g)^2}\left(\frac{E_g}{\omega_a}+\frac{E_g}{\omega_b}\right)^2, \tag{5}$$

with

$$F(\zeta_v)=\left(\zeta_v N_v-\frac{1}{3}N_v^3-\frac{1}{2}N_v^2-\frac{1}{6}N_v\right), \tag{6}$$

where $\zeta_v = (\hbar\omega_a + \hbar\omega_b - E_g)/E_{v,11}$ defines how far the two-photon transition energy is above the bandgap normalized to the linear absorption edge, $E_{v,11} = E_{c,1} + E_{v,1} = \hbar^2\pi^2/(2\mu_{v,\perp}d^2)$, $N_v = \mathrm{Int}(\sqrt{\zeta_v})$ is the number of two-photon transitions between the valence and conduction subbands, α is the fine structure constant, m_0 is the electron mass, μ_v are the reduced effective masses of the bands, and d is the well width. For TM-TM polarized light,

$$\alpha_{2,\perp}(\omega_a;\omega_b)=\frac{16}{3\pi}\frac{\alpha^2 E_p\left(E_{lh,11}\right)^2\mu_{lh,||}\,d}{n_a n_b m_0 E_g^3}\left[\sum_{n=1}^{N_1}F_1(n)+\sum_{n=1}^{N_2}F_2(n)\right]\frac{1}{(\omega_a/E_g)(\omega_b/E_g)^2}, \tag{7}$$

where

$$F_{1(2)}(n)=\left|\left[(2n+1)-\frac{1}{(2n+1)}\right]\left[\frac{\omega_a}{\left[\omega_a-\frac{(1+2n)\pi^2}{2m_{c(lh,\perp)}d^2}\right]\left[\omega_a+\frac{(1+2n)\pi^2}{2m_{lh,\perp(c)}d^2}\right]}+\frac{\omega_b}{\left[\omega_b-\frac{(1+2n)\pi^2}{2m_{c(lh,\perp)}d^2}\right]\left[\omega_b+\frac{(1+2n)\pi^2}{2m_{lh,\perp(c)}d^2}\right]}\right]\right|^2, \tag{8}$$

and

$$N_{1(2)}=Int\left[\left(\zeta_{lh}-\frac{\mu_{lh,\perp}}{m_{c(lh,\perp)}}+\left(\frac{\mu_{lh,\perp}}{m_{c(lh,\perp)}}\right)^2\right)^{1/2}-\frac{\mu_{lh,\perp}}{m_{c(lh,\perp)}}\right], \tag{9}$$

The ND-2PA coefficients may be measured experimentally by pump-probe where the transmission of the weak probe beam at ω_a is monitored in the presence of the strong pump beam at ω_a. Figure 4 shows the calculated ND-2PA coefficient of bulk GaAs and a 10 nm wide QW for TE-TE and TM-TM polarized light with a pump photon energy $\hbar\omega_b = 0.12E_g$ (λ_b = 7.5 μm) and varying the probe photon energy $\hbar\omega_a$. For bulk, α_2 is plotted against the sum of photon energies normalized to the bandgap (E_g), whereas for the QW, the energy is normalized to the respective one-photon absorption threshold ($E_g + E_{hh,11}$ for TE-TE and $E_g + E_{lh,11}$ for TM-TM). The photon energy of the pump is chosen to have a long wavelength to avoid D-2PA or three photon absorption (3PA) from the pump itself. This allows comparison of the ND-2PA coefficient of the bulk and QW on the same scale. At a normalized energy of 1.02, Figure 4(a), $\alpha_{2,||}$ in a 10 nm QW is ~ 2× that of the bulk, and in a 5 nm QW is ~ 3.4× that of the bulk. The continuous increase of $\alpha_{2,||}$ from n^{th} valence band to n^{th} conduction band is due to the linear dependence of the intraband transition matrix elements on the in-plane wave vector ($\mathbf{k}_{||}$), and the signature step-like features of QW's, as seen in linear absorption spectra, is not observed.

At the same normalized energy, $\alpha_{2,\perp}$ in a 10 nm QW is ~ 36× that of the bulk. In the TM-TM case, the onset of 2PA occurs at $\hbar\omega_a + \hbar\omega_b = E_g + E_{lh,12}$, rather than $\hbar\omega_a + \hbar\omega_b = E_g + E_{lh,11}$ as in the TE-TE case, so the sum of the two-photon energies is normalized to $E_g + E_{lh,12}$. The signature step like features of the TM-TM case are due to the selection rules and transition paths that allow intersubband transitions and the fact that the intraband transition matrix elements are independent of $\mathbf{k}_{\|}$.

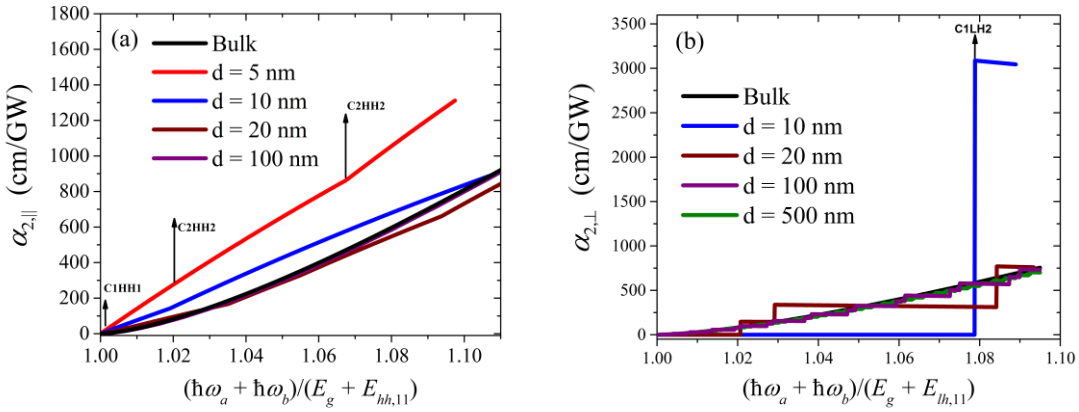

Figure 4. ND-2PA coefficient in bulk GaAs and GaAs QW's of different widths: (a) TE-TE case and (b) TM-TM case.

Since in the TM-TM case the first two-photon transition occurs at $E_g + E_{lh,12}$, the range over which the pump and probe photon energies can vary depends on the QW width, and is limited to a range given by

$$\omega_b > E_{lh,2} - E_{lh,1}, \tag{10}$$

and

$$E_g + E_{lh,12} - \omega_b < \omega_a < E_g + E_{lh,11}. \tag{11}$$

This limitation in pump and probe photon energies is depicted in Figure 5, which describes different scenarios for $\alpha_{2,\perp}$.

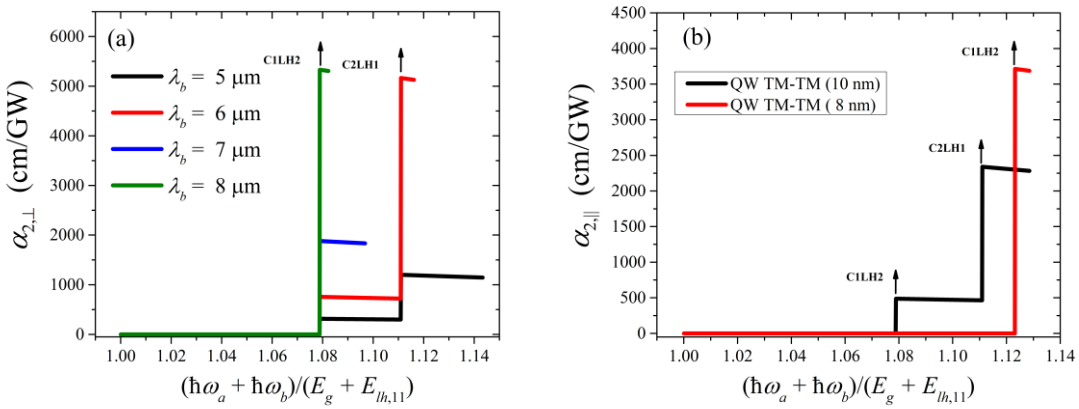

Figure 5. ND-2PA coefficient $\alpha_{2,\perp}$ in a GaAs QW (a) of width 10 nm for various pump photon energies, and (b) of different widths for a constant pump photon energy $\hbar\omega_b$ corresponding to a wavelength of 5.5 μm.

As observed in Figure 5, as we decrease the photon energy $\hbar\omega_b$, we observe a strong increase in $\alpha_{2,\perp}$ at the C1LH2 transition. The C2LH1 transitions are not observed for λ_b = 7 μm and 8 μm because $\hbar\omega_a + \hbar\omega_b = E_g + E_{lh,12}$. This is also observed in Figure 5(b) as we decrease the QW width from 10 nm to 8 nm. As the confinement increases there is a strong enhancement of $\alpha_{2,\perp}$ at the C1LH2 transition, but the C2LH1 transition is not observed for 5.5 μm.

In ND-2PA for bulk semiconductors the enhancement is limited by the density of states and the intraband matrix element, both of which approach zero towards the band edge. In QW's, however, for the TM-TM case, the enhancement

is due to interband and intersubband resonances. These occur when $\hbar\omega_a$ nears $E_g + E_{lh,11}$ (interband) and when $\hbar\omega_b$ approaches $E_{c,2} - E_{c,1}$ or $E_{lh,2} - E_{lh,1}$ (intersubband). But as we approach these resonances, both the transition matrix elements and the density of states remain finite. The density of states is also large near the band edge, which leads to the enhancement of the ND-2PA over that for the bulk semiconductor.

The large enhancement of ND-2PA in QW's is useful for determining the potential of QW's for nonlinear optical devices. One of the applications is mid-IR detection using the strong enhancement of END-2PA in the TM-TM polarization case with the QW's acting as the active region in a photodiode. In addition, inverted QW's may provide two-photon gain and a possible path to a semiconductor two-photon laser.

2.3 Nondegenerate Enhancement of 3PA

Enhancement of three-photon absorption (3PA) is even larger than the orders of magnitude enhancement observed in 2PA since there is an additional photon to give intermediate state resonance enhancement. This provides an extra energy term in the denominator of the 3PA equivalent of Eq. (1). 3PA in semiconductors is well described by application of third-order perturbation theory to Kane's (spin degenerate) four-band model [25-27]. The presence of the various bands, as compared to the simpler two parabolic band model, gives rise to quantum interference between the various pathways, yielding a rich structure to the D-3PA spectra of various zinc-blende semiconductors. Figure 6(a) shows the energy-momentum diagram of Kane's band model, which includes conduction, heavy- and light-hole, split-off bands, along with examples of three different quantum pathways for 3PA. Using such a model at a nondegeneracy of $\hbar\omega_a/\hbar\omega_b$ = 10 yields a predicted enhancement for ND-3PA of 2410× its degenerate value (for the same energy sum), compared to only 150× enhancement for ND-2PA. Experimentally, we have measured enhancement in GaAs via pump-probe techniques, the results of which are shown in Figure 6(b), compared to measurements of D-3PA [28]. We observe significant enhancement using a pump photon energy of 0.16 eV ($0.11E_g$). Such large 3PA coefficients may be important to consider in the design of semiconductor based IR optical parametric devices, and will play a limiting factor in a two-photon semiconductor laser.

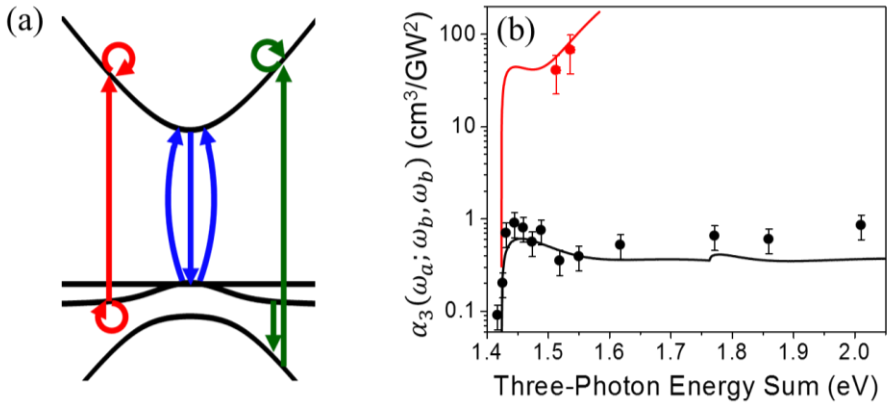

Figure 6. (a) E-k diagram of Kane's (spin-degenerate) 4-band model showing three examples of quantum pathways for 3PA. (b) Comparison of (circles) measured data of GaAs to (solid curves) theory (×3) for both (black) degenerate and (red) nondegenerate (with $\hbar\omega_b$ = 0.16 eV) [28].

3. NONDEGENERATE NONLINEAR REFRACTION

3.1 Nonlinear Kramers-Kronig relations

The NLR dispersion can be calculated from the nonlinear absorption spectrum using Kramers-Kronig (KK) transformations by

$$n_2(\omega_a,\omega_b)=\frac{2}{\pi}\int_0^\infty \frac{\alpha_{NL}(\omega,\omega_b)}{\omega^2-\omega_a^2}\,\mathrm{d}\omega, \tag{12}$$

where α_{NL} includes 2PA as well as the stimulated Raman and optical Stark effects. Figure 7(a) illustrates these contributions for the degenerate case of ZnO. In spectral regions well below linear absorption resonances, the 2PA contribution dominates the dispersion of n_2 which grows from low frequencies to a maximum near the onset of 2PA and

then turns negative as the photon energy approaches the bandgap. The Raman and Stark effects give overall minor contributions in positive and negative ways, respectively, and only become resonant at the bandgap [16]. The nondegenerate dispersion of $n_2(\omega_a; \omega_b)$ can also be predicted from the ND-2PA spectrum via KK calculations. Fig. 3(b) shows the predicted $n_2(\omega_a; \omega_b)$ dispersion by fixing $\hbar\omega_b$ at a certain percentage of E_g and varying $\hbar\omega_a$ from 0 to E_g. Owing to the large enhancement of $\alpha_2(\omega_a; \omega_b)$, $n_2(\omega_a; \omega_b)$ is also positively enhanced near the 2PA edge with increasing nondegeneracy and becomes significantly larger than its degenerate counterpart. Particularly for the END case, $\hbar\omega_b \rightarrow 0.1E_g$, $n_2(\omega_a; \omega_b)$ becomes anomalously dispersive near the bandgap and rapidly switches sign from positive to negative over a very narrow spectral range.

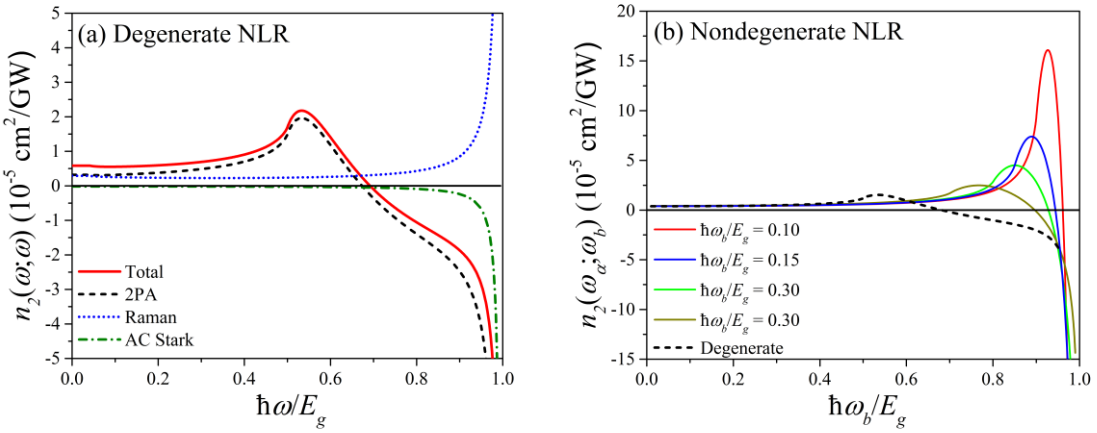

Figure 7. (a) Theory of degenerate n_2 of ZnO with total NLR (solid line) decomposed into 2PA, Raman and AC Stark mechanisms (dash line) [16]; (b) calculated nondegenerate enhancement of NLR of ZnO (solid lines), for various pump energies, compared to the degenerate case (dash line) [18].

3.2 Experiment and discussion

We apply our recently developed ultrafast beam deflection (BD) technique [19, 29, 30] to measure the ND-NLR of several direct-gap semiconductors. The experimental setup and beam geometries are shown in Figure 8(a). Beam deflection is an excite-probe technique using fs pulses, where an infrared excitation pulse creates an index gradient that follows its spatial Gaussian profile. The probe beam at another wavelength is focused ~ 5× smaller than the excitation and is spatially displaced to the Gaussian wings off the excitation's center. The index gradient is nearly linear near where the gradient is maximized. Therefore, the probe is deflected by a small angle which can be measured using a quad-segmented detector by taking the difference of the energy falling on the left and right halves $\Delta E = E_{left} - E_{right}$ and normalizing to the total energy E. The BD signal, $\Delta E/E$, is proportional to $n_2(\omega_a; \omega_b)$.

Figure 8(b) shows agreement between the measured and theoretical nondegenerate $n_2(\omega_a; \omega_b)$ for ZnO, as compared to the calculated degenerate counterpart. We use a Ti:sapphire amplified laser system (Coherent Legend Elite Duo HE+) producing 12 mJ, ~40 fs (FWHM) pulses at a 1 kHz repetition rate to pump an optical parametric amplifier (TOPAS-HE) to produce the excitation pulses at 1440 nm. A portion of the excitation is then used to produce a white-light continuum (WLC) in a 5 mm thick sapphire crystal, from which narrow bandpass filters select the desired wavelength. A 1 mm thick fused silica sample is measured for calibration at all wavelength combinations. We observe an increase of $n_2(\omega_a; \omega_b)$ approaching the 2PA edge. Particularly, at a probe wavelength of 480 nm ($0.81E_g$) where 2PA starts, $n_2(\omega_a; \omega_b)$ is enhanced 7× over the zero frequency limit and 1.8× over its degenerate counterpart with this moderate nondegeneracy ($\hbar\omega_b = 0.26E_g$). We have measured a much larger enhancement with excitation photon energy $\hbar\omega_b = 0.16E_g$. The theoretical prediction using the KK transformation agrees with both the dispersion relation and the magnitude of nondegenerate NLR when using experimental best fit parameter of the two-band model [16].

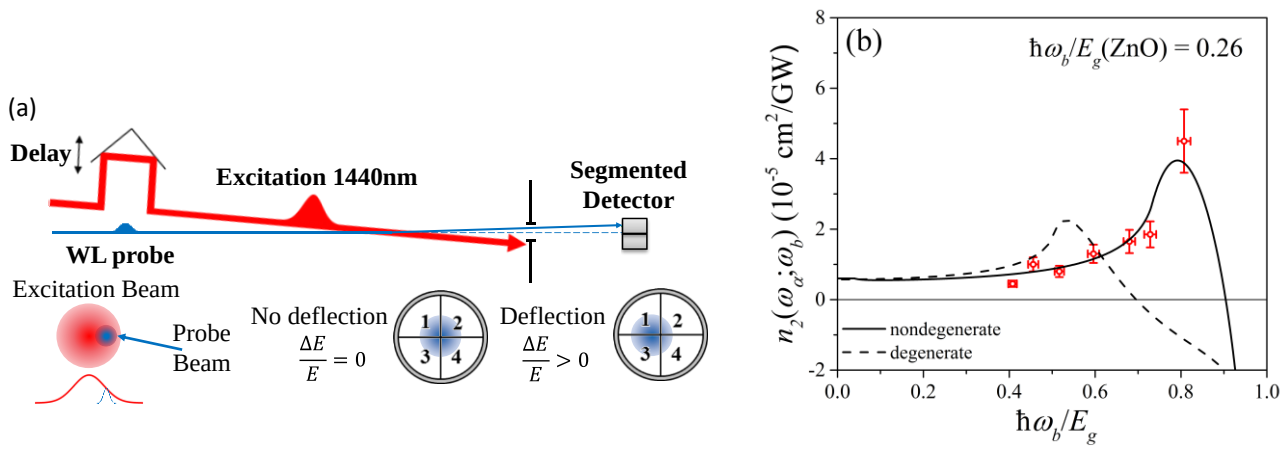

Figure 8. (a) The nondegenerate beam deflection measurement setup including excitation and probe overlap geometry and position sensitive quad-segmented photodetector. (b) Experimental data of $n_2(\omega_a; \omega_b)$ of ZnO (square), along with a theoretical calculations of degenerate (dash curve) and nondegenerate (solid curve) NLR.

In the END case, this enhanced n_2 may impact numerous applications such as all-optical switching, and the rapid anomalous nonlinear dispersion will provide large modulation of a femtosecond pulse with narrow bandwidth centered near the zero crossing frequency which may enable other new applications such as nonlinear pulse shaping.

4. CONCLUSION

Nondegenerate nonlinearities in semiconductors are orders of magnitude greater than those in the degenerate case, and yet remain largely underexplored. This enhancement is due to intermediate state resonance enhancement, coupled with the semiconductor band structure, which provides the largest enhancements for extremely different photon energies. Such enhancements offer great potential for a host of applications, from gated detection of mid-IR pulses and 3D-IR imaging, to all-optical switching for communication, to the potential for two-photon semiconductor lasers.

REFERENCES

1. A. Rostami, "Low threshold and tunable all-optical switch using two-photon absorption in array of nonlinear ring resonators coupled to MZI," Microelectr. J. **37**(9), 976-981 (2006).
2. S. M. Hendrickson, C. N. Weiler, R. M. Camacho, P. T. Rakich, A. I. Young, M. J. Shaw, T. B. Pittman, J. D. Franson, and B. C. Jacobs, "All-optical-switching demonstration using two-photon absorption and the Zeno effect," Phys. Rev. A **87**(2), 023808 (2013).
3. H. K. Tsang, R. S. Grant, R. V. Penty, I. H. White, J. B. D. Soole, E. Colas, H. P. Leblanc, N. C. Andreadakis, M. S. Kim, and W. Sibbett, "GaAs/GaAlAs multiquantum well waveguides for all-optical switching at 1.55 mu m," Electron. Lett. **27**(22), 1993-1995 (1991).
4. G. I. Stegeman, and E. M. Wright, "All-optical waveguide switching," Opt. Quant. Electron. **22**(2), 95-122.
5. E. W. Van Stryland, Y. Y. Wu, D. J. Hagan, M. J. Soileau, and K. Mansour, "Optical limiting with semiconductors," J. Opt. Soc. Am. B **5**(9), 1980-1988 (1988).
6. E. W. Van Stryland, H. Vanherzeele, M. A. Woodall, M. J. Soileau, A. L. Smirl, S. Guha, and T. F. Boggess, "Two Photon Absorption, Nonlinear Refraction, And Optical Limiting In Semiconductors," Opt. Eng. **24**(4), 244613-244613- (1985).
7. D. A. Fishman, C. M. Cirloganu, S. Webster, L. A. Padilha, M. Monroe, D. J. Hagan, and E. W. Van Stryland, "Sensitive mid-infrared detection in wide-bandgap semiconductors using extreme non-degenerate two-photon absorption," Nat. Photon. **5**(9), 561-565 (2011).
8. H. S. Pattanaik, D. A. Fishman, E. W. Van Stryland, and D. J. Hagan, "Pulsed and CW IR Detection in Wide-gap Semiconductors using Extremely Nondegenerate Two-photon Absorption," in *CLEO: 2013*(Optical Society of America, San Jose, California, 2013), p. CTu3E.3.
9. H. S. Pattanaik, M. Reichert, D. J. Hagan, and E. W. Van Stryland, "Three-dimensional IR imaging with uncooled GaN photodiodes using nondegenerate two-photon absorption," Opt. Express **24**(2), 1196-1205 (2016).
10. J. H. Yu, S.-H. Kwon, Z. Petrášek, O. K. Park, S. W. Jun, K. Shin, M. Choi, Y. I. Park, K. Park, H. B. Na, N. Lee, D. W. Lee, J. H. Kim, P. Schwille, and T. Hyeon, "High-resolution three-photon biomedical imaging using doped ZnS nanocrystals," Nat. Mater. **12**(4), 359-366 (2013).

11. B. S. Chris, B. André, and M. Eric, "Laser-induced breakdown and damage in bulk transparent materials induced by tightly focused femtosecond laser pulses," Meas. Sci. Technol. **12**(11), 1784 (2001).
12. M. Göppert-Mayer, "Über Elementarakte mit zwei Quantensprüngen," Ann. Phys. **401**(3), 273-294 (1931).
13. D. C. Hutchings, M. Sheik-Bahae, D. J. Hagan, and E. W. Stryland, "Kramers-Krönig relations in nonlinear optics," Opt Quant Electron **24**(1), 1-30 (1992).
14. R. W. Boyd, *Nonlinear Optics* (Academic, 2008).
15. G. I. Stegeman, and R. A. Stegeman, *Nonlinear Optics: Phenomena, Materials and Devices* (John Wiley & Sons, Inc., Hoboken, NJ, 2012).
16. M. Sheik-Bahae, D. C. Hutchings, D. J. Hagan, and E. W. Van Stryland, "Dispersion of bound electron nonlinear refraction in solids," IEEE J. Quant. Electron. **27**(6), 1296-1309 (1991).
17. H. S. Pattanaik, M. Reichert, J. B. Khurgin, D. J. Hagan, and E. W. V. Stryland, "Enhancement of Two-Photon Absorption in Quantum Wells for Extremely Nondegenerate Photon Pairs," IEEE J. Quant. Electron. **52**(3), 9000114 (2016).
18. M. Sheik-Bahae, J. Wang, and E. W. Van Stryland, "Nondegenerate optical Kerr effect in semiconductors," IEEE J. Quant. Electron. **30**(2), 249-255 (1994).
19. M. R. Ferdinandus, H. Hu, M. Reichert, D. J. Hagan, and E. W. Van Stryland, "Beam deflection measurement of time and polarization resolved ultrafast nonlinear refraction," Opt. Lett. **38**(18), 3518-3521 (2013).
20. C. M. Cirloganu, L. A. Padilha, D. A. Fishman, S. Webster, D. J. Hagan, and E. W. Van Stryland, "Extremely nondegenerate two-photon absorption in direct-gap semiconductors [Invited]," Opt. Express **19**(23), 22951-22960 (2011).
21. M. Reichert, A. L. Smirl, G. Salamo, D. J. Hagan, and E. W. Van Stryland, "Observation of Nondegenerate Two-Photon Gain in GaAs," arXiv:1602.05912 (2016).
22. H. N. Spector, "Two-photon absorption in semiconducting quantum-well structures," Phys. Rev. B **35**(11), 5876-5879 (1987).
23. A. Pasquarello, and A. Quattropani, "Gauge-invariant two-photon transitions in quantum wells," Phys. Rev. B **38**(9), 6206-6210 (1988).
24. J. B. Khurgin, "Nonlinear response of the semiconductor quantum-confined structures near and below the middle of the band gap," J. Opt. Soc. Am. B **11**(4), 624-631 (1994).
25. E. O. Kane, "Band structure of indium antimonide," J. Phys. Chem. Solids **1**(4), 249-261 (1957).
26. S. L. Chuang, *Physics of Optoelectronic Devices* (Wiley-Interscience, New York, 1995).
27. C. M. Cirloganu, P. D. Olszak, L. A. Padilha, S. Webster, D. J. Hagan, and E. W. Van Stryland, "Three-photon absorption spectra of zinc blende semiconductors: theory and experiment," Opt. Lett. **33**(22), 2626-2628 (2008).
28. D. Peceli, "Absorptive and Refractive Optical Nonlinearities in Organic Molecules and Semiconductors," in *CREOL, The College of Optics and Photonics*(University of Central Florida, 2013), p. 210.
29. M. Reichert, H. Hu, M. R. Ferdinandus, M. Seidel, P. Zhao, T. R. Ensley, D. Peceli, J. M. Reed, D. A. Fishman, S. Webster, D. J. Hagan, and E. W. Van Stryland, "Temporal, spectral, and polarization dependence of the nonlinear optical response of carbon disulfide," Optica **1**(6), 436-445 (2014).
30. M. Reichert, P. Zhao, J. M. Reed, T. R. Ensley, D. J. Hagan, and E. W. Van Stryland, "Beam deflection measurement of bound-electronic and rotational nonlinear refraction in molecular gases," Opt. Express **23**(17), 22224-22237 (2015).